



1 **Ozone affected by a succession of four landfall typhoons in**  
2 **the Yangtze River Delta, China: major processes and health**  
3 **impacts**

4 Chenchao Zhan <sup>a,1</sup>, Min Xie <sup>a,\*</sup>, Chongwu Huang <sup>a,1</sup>, Tijian Wang <sup>a</sup>, Jane Liu <sup>b,c</sup>, Meng Xu <sup>d</sup>, Chaoqun  
5 Ma <sup>a</sup>, Jianwei Yu <sup>e</sup>, Yumeng Jiao <sup>f</sup>, Mengmeng Li <sup>a</sup>, Shu Li <sup>a</sup>, Bingliang Zhuang <sup>a</sup>, Ming Zhao <sup>a</sup>,  
6 Dongyang Nie <sup>a</sup>

7 <sup>a</sup> School of Atmospheric Sciences, Joint Center for Atmospheric Radar Research of CMA/NJU,  
8 CMA-NJU Joint Laboratory for Climate Prediction Studies, Jiangsu Collaborative Innovation  
9 Center for Climate Change, Nanjing University, Nanjing 210023, China

10 <sup>b</sup> College of Geographic Sciences, Fujian Normal University, 350007, Fuzhou, China

11 <sup>c</sup> Department of Geography and Planning, University of Toronto, Toronto, Ontario, Canada

12 <sup>d</sup> Jiangsu Provincial Climate Center, Nanjing 210009, China

13 <sup>e</sup> Jiangsu Provincial Meteorological Observatory, Nanjing 210008, China

14 <sup>f</sup> Department of Microbiology and Parasitology, Bengbu Medical College, Bengbu 233030, China

15 -----

16 \* Corresponding author. minxie@nju.edu.cn (M. Xie)

17 <sup>1</sup> The third author can be considered as the co-first author

18

19 **Abstract:** Landfall typhoon can significantly affect O<sub>3</sub> in the Yangtze River Delta (YRD) region. In  
20 this study, we investigate a unique case characterized by two multiday regional O<sub>3</sub> pollution  
21 episodes related to four successive landfall typhoons in the summer of 2018 in the YRD. The results  
22 show that O<sub>3</sub> pollution episodes mainly occurred during the period from the end of typhoon and the  
23 arrival of the next typhoon. The moment that typhoon reached the 24-h warning line and the last  
24 moment of typhoon activity in the mainland China can be roughly regarded as time nodes.  
25 Meanwhile, the variations of O<sub>3</sub> was related to the track, duration and landing intensity of the  
26 typhoons. The impact of typhoon on O<sub>3</sub> was like a wave superimposed on the background of high  
27 O<sub>3</sub> concentration in the YRD in summer. When typhoon was near the 24-h warning line before it  
28 landed the coast line of the YRD, the prevailing wind originally from the ocean changed to from the  
29 inland, and transported lots of precursors from the polluted areas to the YRD. With typhoon, the low  
30 temperature, strong upward airflows, more precipitation and wild wind prevented high O<sub>3</sub> episodes.



31 After typhoon, the air below the 700 hPa atmospheric layer was warm and dry, which was  
32 conducive to the formation of O<sub>3</sub> from the abundance of precursors. It is note-worthy that O<sub>3</sub> is  
33 mainly generated in the middle of boundary layer (~ 1000 m), and then transported to the surface  
34 by downward airflows or turbulences. Moreover, O<sub>3</sub> can be accumulated and trapped on the ground  
35 due to the poor diffusion conditions because the vertical diffusion and horizontal diffusion were  
36 suppressed by downward airflows and light wind, respectively. The premature mortalities attributed  
37 to O<sub>3</sub> exposure in the YRD during the study period is 194.0, more than the casualties caused directly  
38 by the typhoons. This work enhances our understanding of how landfall typhoons affect O<sub>3</sub> in the  
39 YRD, which can be helpful to forecast the O<sub>3</sub> pollution synthetically impacted by the subtropical  
40 high and typhoon.

41 **Key Words:** ozone; landfall typhoon; the Yangtze River Delta region;

42

## 43 1 Introduction

44 The tropospheric ozone (O<sub>3</sub>), which is formed by a series of complex photochemical reactions  
45 between volatile organic compounds (VOCs) and nitrogen oxides (NO<sub>x</sub>=NO+NO<sub>2</sub>) in combination  
46 with sunlight (Chameides and Walker, 1973; Xie et al., 2014), has received continuous attention due  
47 to its negative impact on air quality (Chan and Yao, 2008; Monks et al., 2015), human health (Jerrett  
48 et al., 2009), climate (Allen et al., 2012; IPCC, 2014) and biosphere (Dingenen et al., 2009).  
49 Research on urban O<sub>3</sub> pollution can date back to the early 1950s, beginning with the Los Angeles  
50 smog. In China, the photochemical smog, which is characterized by high level of O<sub>3</sub>, was first  
51 discovered in Xigu district of Lanzhou in 1970s (Tang et al., 1989). However, with the key  
52 atmospheric environmental problem was coal-smoke pollution (such as acid rain) at that time (Wang  
53 et al., 2019), little systematic research and coordinated O<sub>3</sub> monitoring were performed in China until  
54 the mid-2000s (Wang et al., 2017).

55 Since the beginning of 21st century, the complex air pollution, which is dominated by fine  
56 particulate matter (PM<sub>2.5</sub>, particles of 2.5 microns or less in aerodynamic diameter) and surface O<sub>3</sub>,  
57 has been ingrained in the megacities of China (Chan and Yao, 2008; Jin et al., 2016; Kan et al.,  
58 2012). Air pollution has evolved into a political and economic concern in China. Due to drastic air  
59 pollution control since 2013, particle pollution has been greatly reduced, appearing a significantly  
60 decrease in sulfur dioxide (SO<sub>2</sub>), NO<sub>x</sub> and PM<sub>2.5</sub>. However, the concentrations of O<sub>3</sub> and VOCs had



61 an increase from 2013 to 2017 ( Li et al., 2017), suggesting that more attention should be paid to  
62 controlling O<sub>3</sub> and VOCs in the future. Overall, the causes of air pollution and the control policies  
63 are still a major challenge in China, especially in understanding the sources, transport and dispersion  
64 processes, and chemical formation mechanisms of O<sub>3</sub> and its precursors (Ding et al., 2016; Guo et  
65 al., 2014; Huang et al., 2014).

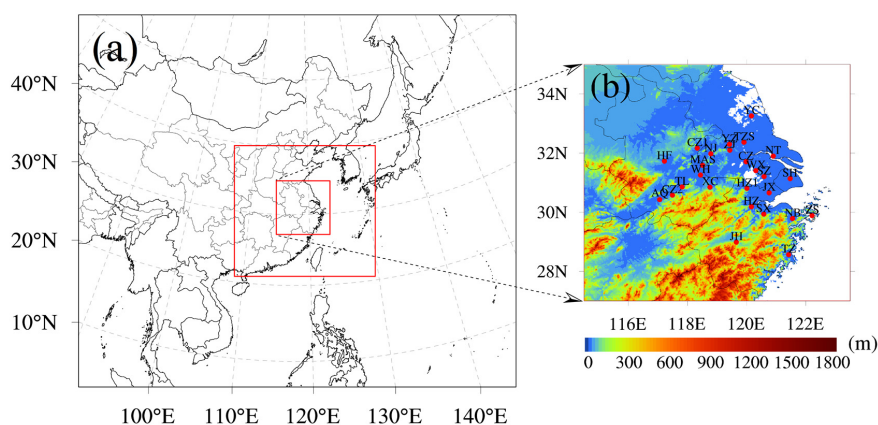
66 Typhoon (tropical cyclone, TC) is one of the most important factors of natural disasters in East  
67 Asia. Out of the total provinces in China, 10 coastal and 6 island provinces are affected by typhoon  
68 induced disasters, with more than 250 million lives are affected (Liu et al., 2009). The average  
69 number of typhoons making landfall in China is 9 each year, and those typhoons usually inflict vast  
70 losses in human life and property due to the accompanied strong wind, torrential rains and huge  
71 storm surges (Zhang et al., 2009; Zhao et al., 2012). Because of the long lifetime and tremendous  
72 energy, typhoon has a significantly influence on local atmospheric conditions, and thereby can affect  
73 surface O<sub>3</sub> concentration through advection, diffusion, deposition and other processes. The impact  
74 of typhoon on O<sub>3</sub> has attracted extensive attention in recent years (Deng et al., 2019; Huang et al.,  
75 2005; Shu et al., 2016; Wang and Kwok, 2002; Wei et al., 2016; Yang et al., 2012). For example,  
76 Deng et al. (2019) reported that high O<sub>3</sub> and high aerosol concentrations (double high episodes) are  
77 likely to occur when the PRD is under the control of typhoon periphery and subtropical high with  
78 strong downdrafts. Previous studies were mainly in the southern China (including Hong Kong and  
79 Taiwan), where are frequently affected by typhoons. However, research on the impact of landfall  
80 typhoons on O<sub>3</sub> is still limited.

81 The Yangtze River Delta (YRD) region, being one of the most developed and densely  
82 populated regions in China, is located on the western coast of the Pacific Ocean. With 3.7% of the  
83 area and 16.0% of the population of China, the YRD contributed over 20% of the national total  
84 Gross Domestic Product (GDP) in 2019. Due to the rapid economic development and high energy  
85 consumption, this region is suffering from intense air pollution (Ding et al., 2013; Li et al., 2019;  
86 Wang et al., 2015; Xie et al., 2016). In 2017, the 90th percentile of the maximum daily 8-hour  
87 average (MDA8) O<sub>3</sub> concentration was 170 µg m<sup>-3</sup>, and 16 of the 26 cities (Figure 1b) in the YRD  
88 failed to meet national standard ([http://www.cnemc.cn/jcbg/zghjzkgb/201905/t20190529\\_704755.html](http://www.cnemc.cn/jcbg/zghjzkgb/201905/t20190529_704755.html)). Therefore, it is an urgent task to investigate the spatiotemporal characteristic of O<sub>3</sub> as well as  
89 its formation mechanism in the YRD. Influenced by monsoon weather, the warm and stagnation  
90



91 conditions play an important role in the occurrence of high-level O<sub>3</sub> in summer (Li et al., 2018; Liao  
92 et al., 2015; Lu et al., 2018; Zhao et al., 2010). Synoptic weather systems, such as typhoon and cold  
93 front, also have significant effects on O<sub>3</sub> in the YRD (Hu et al., 2013; Shu et al., 2016). This work  
94 aims to reveal the main processes of landfall typhoon affecting surface O<sub>3</sub> in the YRD, hoping to  
95 fill the knowledge gap and be helpful for making reasonable pollution control measures.

96 In this study, we report an outstanding case observed in the YRD during the period from 16  
97 July to 25 August, during which multiday episode of high O<sub>3</sub> occurred and was related to four  
98 successive landfall typhoons. Base on the monitoring data and numerical simulation, we further  
99 explore the impact of landfall typhoons on O<sub>3</sub> in the YRD, including the major processes and health  
100 impacts. The following part of this paper is structured as the follows: Section 2 gives a brief  
101 description of monitoring data, the analysis methods, and model configurations. The results as well  
102 as the discussions are detailed in section 3. Section 4 summarizes the main conclusions.  
103



104  
105 **Figure 1. The three nested modeling domains (a) in WRF, and the locations of 26 typical cities**  
106 **in the YRD with terrain elevation data (b). The cities in (b) include: Nanjing (NJ), Wuxi (WX),**  
107 **Changzhou (CZ), Suzhou (SZ), Nantong (NT), Yancheng (YC), Yangzhou (YZ), Zhenjiang (ZJ)**  
108 **and Taizhoushi (TZS) located in Jiangsu province; Hangzhou (HZ), Ningbo (NB), Jiaxing (JX),**  
109 **Huzhou (HZ1), Shaoxing (SX), Jinhua (JH), Zhoushan (ZS) and Taizhou (TZ) located in**  
110 **Zhejiang province; Hefei (HF), Wuhu (WH), Maanshan (MAS), Tongling (TL), Anqing (AQ),**  
111 **Chuzhou (CZ1), Chizhou (CZ2) and Xuancheng (XC) located in Anhui province; and the**



112 megacity Shanghai (SH). The terrain elevation data are available at  
113 [https://www.ngdc.noaa.gov/mgg/global/relief/ETOPO1/data/bedrock/cell\\_registered/netcdf/](https://www.ngdc.noaa.gov/mgg/global/relief/ETOPO1/data/bedrock/cell_registered/netcdf/).

114

## 115 **2 Data and methods**

### 116 **2.1 Air quality data**

117 Surface air pollutants monitored by the China National Environmental Monitoring Center  
118 (CNMC) Network are used in this study. The nationwide observation network began operating in  
119 74 major cities in 2013, and it included 1597 nonrural sites covering 454 cities by 2017 (Lu et al.,  
120 2018). The monitoring data are strictly in accordance with the national monitoring regulations  
121 (<http://www.cnemc.cn/jcgf/dqhj/>), and can be acquired from the national urban air quality real-time  
122 publishing platform (<http://106.37.208.233:20035/>). Each monitoring site automatically measures  
123 hourly air pollutants (PM<sub>2.5</sub>, PM<sub>10</sub>, SO<sub>2</sub>, NO<sub>2</sub>, O<sub>3</sub> and CO), and the urban hourly pollutants are  
124 calculated by averaging the pollutants measured at all monitoring sites in that city. The MDA8 O<sub>3</sub>  
125 is calculated based on the hourly O<sub>3</sub> with more than 18-h measurements (Liao et al., 2017). Manual  
126 inspection, including the identification and handling of invalid and lacking data, is performed  
127 following previous studies (Xie et al., 2016; Shu et al., 2017; Zhan et al., 2019).

### 128 **2.2 Surface and sounding meteorological data**

129 With respect to surface observed meteorological data, stations at the three provincial capital  
130 cities (Nanjing, Hangzhou and Hefei) and the megacity Shanghai are selected, which are ZSNJ  
131 (32.00°N, 118.80°E), ZSHC (30.23°N, 120.17°E), ZSOF (31.87°N, 117.23°E) and ZSPD (31.12°N,  
132 121.77°E), respectively. These surface observations, including 2-m temperature, 10-m wind speed  
133 and direction and 2-m relative humidity, are recorded hourly and can be obtained from the website  
134 of the University of Wyoming (<http://weather.uwyo.edu/surface/>).

135 To verify the upper-air fields, the sounding observations at Shanghai (31.40°N, 121.46°E) and  
136 Nanjing (32.00°N, 118.80°E) are used. These sounding observations (pressure, temperature, relative  
137 humidity, wind direction and wind speed etc.) are also acquired from the website of the University  
138 of Wyoming (<http://weather.uwyo.edu/upperair/sounding.html>), with a time resolution of 12 h  
139 (00:00 and 12:00 UTC).

### 140 **2.3 The best-track TC dataset**

141 To capture the characteristics of landfall typhoons, the best-track TC dataset issued by the



142 China Meteorological Center (CMA) is considered due to its good performance on the landfall  
143 typhoons in the mainland China (available at [http://tcdata.typhoon.org.cn/zjljsjj\\_sm.html](http://tcdata.typhoon.org.cn/zjljsjj_sm.html)). The  
144 dataset covers seasons from 1949 to the present, the region north of the equator and west of 180°E,  
145 and is updated annually (Li and Hong, 2016; Ying et al., 2014). A wealth of information on typhoon  
146 is recorded every 6h in the dataset, including location, minimum sea level pressure, etc. For landfall  
147 typhoons, 24h before they land and during their activities in the mainland China, the data will be  
148 recorded every 3h. Refer to the national standard for grade of tropical cyclones (GB/T 19201-2006),  
149 the intensity category (IC) of tropical cyclones is given in the dataset, which is based on the near  
150 surface maximum 2-min mean wind speed near the tropical cyclone center, ranges from 1 to 6 (Table  
151 1).

152

153 **Table 1. The intensity category of tropical cyclones**

Intensity category (IC)	The near surface maximum 2-min mean wind speed near the tropical cyclone center (m/s)	Beaufort scale
Tropical depression (IC=1)	10.8-17.1	6-7
Tropical storm (IC=2)	17.2-24.4	8-9
Severe tropical storm (IC=3)	24.5-32.6	10-11
Typhoon (IC=4)	32.7-41.4	12-13
Severe typhoon (IC=5)	41.5-50.9	14-15
Super typhoon (IC=6)	≥ 51.0	≥16

154

#### 155 **2.4 Model description and configurations**

156 To simulate the high O<sub>3</sub> episodes over the YRD during the period with typhoons, the WRF-  
157 CMAQ one-way coupled model is applied, which consists of WRF v3.6.1  
158 (<https://www2.mmm.ucar.edu/wrf/users/>) developed by the United States National Center for  
159 Atmospheric Research (NCAR) and CMAQ v5.0.2 (<https://github.com/USEPA/CMAQ/tree/5.0.2>)  
160 developed by the United States Environmental Protection Agency (EPA).

161 WRF generates offline meteorological inputs for CMAQ with initial and boundary conditions  
162 from the National Centers for Environmental Prediction (NCEP) global final analysis fields every



163 6 h at a spatial resolution of  $1^\circ \times 1^\circ$  (<https://rda.ucar.edu/datasets/ds083.2/>). Three nested domains  
164 are used, with horizontal resolutions of 81, 27 and 9 km, and grids of  $88 \times 75$ ,  $85 \times 79$  and  $97 \times 97$ ,  
165 respectively (Figure 1a). There are 24 vertical sigma layers from surface to 100 hPa, with about 8  
166 layers located below 1.5 km to resolve the boundary layer processes. Furthermore, the major  
167 physical options for the dynamic parameterization in WRF are summarized in Table 2.

168

169 **Table 2. The domains and physical options for WRF in this study**

Items	Contents
Dimensions (x, y)	(88, 75), (85, 79), (97, 97)
Grid spacing (km)	81, 27, 9
Microphysics	WRF Single-Moment 5-class scheme (Hong et al., 2004)
Longwave radiation	RRTM scheme (Mlawer et al., 1997)
Shortwave radiation	Goddard scheme (Kim and Wang, 2011)
Surface layer	Moni-Obukhov scheme (Monin and Obukhov, 1954)
Land-surface layer	Noah land-surface model (Chen and Dudhia, 2001)
Planetary boundary layer	YSU scheme (Hong et al., 2006)
Cumulus parameterization	Grell-Devenyi ensemble scheme (Grell and Devenyi, 2002)

170

171 Since the horizontal domains of CMAQ are one grid smaller than WRF, all three nested  
172 domains are adjusted automatically. The vertical layers of CMAQ are the same as WRF. The  
173 Meteorology Chemistry Interface Processor (MCIP) can convert WRF outputs to the necessary  
174 meteorological inputs for CMAQ. Moreover, the CB05 gas-phase mechanism with aqueous/cloud  
175 chemistry is selected in the CMAQ configurations.

176 The anthropogenic emissions are from the Multi-resolution Emission Inventory for China  
177 (MEIC) in 2016 with the resolution of  $0.25^\circ$  (<http://meicmodel.org/>), including anthropogenic  
178 emissions from power generation, industry, agriculture, residential and transportation sectors. All  
179 emission estimates are spatially allocated to the relevant grid cells based on the meteorological fields  
180 obtained from WRF, and are temporally distributed on an hourly basis. The simulation starts from  
181 00:00 UTC on 13 July to 00:00 UTC 27 August, with the first 72 h as spin-up time.



## 182 2.5 Integrated process rate (IPR) analysis

183 To quantify the contributions of individual processes in O<sub>3</sub> formation, the IPR analysis  
184 provided in the CMAQ is utilized. The IPR analysis can illustrate the contributions to changes in  
185 pollutant concentrations from seven different types of processes, including horizontal advection  
186 (HADV), vertical advection (ZADV), horizontal diffusion (HDIF), vertical diffusion (VDIF), dry  
187 deposition (DDEP), cloud processes with the aqueous chemistry (CLDS) and chemical reaction  
188 process (CHEM), with a mass conservation adjustment at each model grid cell. The IPR analysis  
189 has been widely applied to investigate regional air pollution (Fan et al., 2015; Li et al., 2012; Wang  
190 et al., 2010). In this study, MADV is defined as the sum of HADV and ZADV, and TDIF is defined  
191 as the sum of HDIF and VDIF.

## 192 2.6 Model evaluation

193 To evaluate the model performance, the simulation results in the innermost domain, including  
194 O<sub>3</sub> concentration, air temperature at 2 m (T<sub>2</sub>), relative humidity (RH), wind speed at 10 m (WS<sub>10</sub>)  
195 and wind direction at 10 m (WD<sub>10</sub>), are examined against the hourly observations at the  
196 representative cities (Table 3). The statistical metrics, including correlation coefficient (R), root-  
197 mean-square error (RMSE) and normalized mean bias (NMB), are used in this study. They are  
198 defined as follows:

$$199 \quad R = \frac{\sum_{i=1}^N (S_i - \bar{S})(O_i - \bar{O})}{\sqrt{\sum_{i=1}^N (S_i - \bar{S})^2} \sqrt{\sum_{i=1}^N (O_i - \bar{O})^2}}, \quad (3)$$

$$200 \quad RMSE = \sqrt{\frac{\sum_{i=1}^N (S_i - O_i)^2}{N}}, \quad (4)$$

$$201 \quad NMB = \frac{\sum_{i=1}^N (S_i - O_i)}{\sum_{i=1}^N O_i} \times 100\%, \quad (5)$$

202 where S<sub>i</sub> and O<sub>i</sub> are the simulations and observations, respectively. N is the total number of valid  
203 data.  $\bar{S}$  and  $\bar{O}$  are the average value of simulations and observations. In general, the model results  
204 are acceptable if the values of R, RMSE and NMB are close to 1, 0 and 0, respectively (Li et al.,



205 2017; Shu et al., 2016; Xie et al., 2016).

## 206 **2.7 Estimate of health impacts**

207 Previous studies showed that surface O<sub>3</sub> pollution can induce a series of adverse health impacts  
208 by causing the incidence and mortality of respiratory diseases (Ghude et al., 2016; Jerrett et al.,  
209 2009; Lelieveld et al., 2015). To arouse more attention on the issue that O<sub>3</sub> can be significantly  
210 affected by typhoons in the YRD, we further estimate the premature mortality attributed to O<sub>3</sub> during  
211 the study period.

212 A standard damage function (Anenberg et al., 2010; Liu et al., 2018; Voorhees et al., 2014;  
213 WS/T 666-2019, Technical specifications for health risk assessment of ambient air pollution of  
214 China) is employed to quantify premature mortality due to O<sub>3</sub> exposure:

$$215 \Delta M = y_0 \left( \frac{RR - 1}{RR} \right) \text{Pop}, \quad (1)$$

216 where  $\Delta M$  is the excess mortalities attribute to O<sub>3</sub> exposure,  $y_0$  is the baseline mortality rate, RR is  
217 relative risk and  $(RR-1)/RR$  is the attributable fraction, and Pop is the exposed population. RR can  
218 be calculated using the following relationship:

$$219 RR = \exp(\beta(C - C_0)), \quad (2)$$

220 where  $\beta$  is the concentration-response factor, C is the exposure concentration and  $C_0$  represents the  
221 theoretical minimum-risk concentration.

222 In this study, the mortality rate for respiratory disease is obtained from China Health and  
223 Family Planning Statistical Yearbook 2018 ([https://www.yearbookchina.com/navibooklist-  
224 n3018112802-1.html](https://www.yearbookchina.com/navibooklist-n3018112802-1.html)), which is 68.02/100000. The  $\beta$  is generated from Dong et al. (2016), that is  
225 0.461%. The population data are obtained from the bureau of statistics of different cities in the YRD.  
226 The  $C_0$  is 70  $\mu\text{g m}^{-3}$  for MDA8 O<sub>3</sub> given by the World Health Organization (WHO).

227

## 228 **3 Results and discussions**

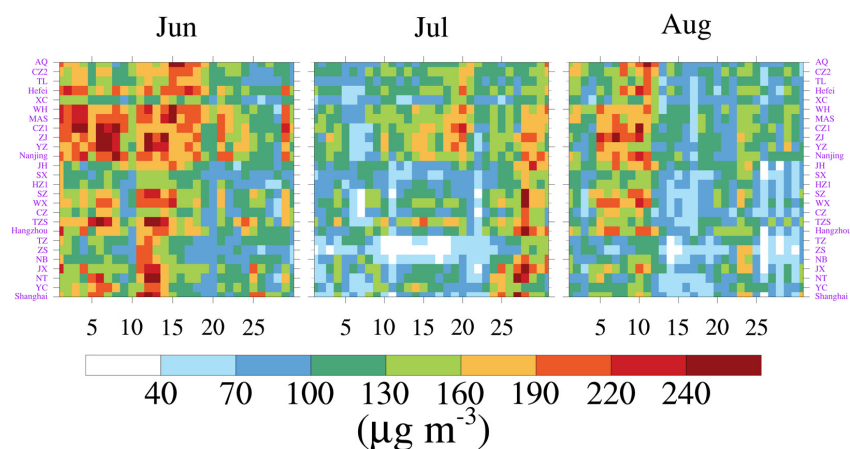
### 229 **3.1 Characteristic of O<sub>3</sub> episodes**

230 In the midsummer season, the warm sea surface (high temperature) is conducive to the  
231 generation of typhoon (high O<sub>3</sub> concentration), which provides a good opportunity to investigate  
232 the mechanism of typhoon affecting O<sub>3</sub> in the YRD. Figure 2 shows the MDA8 O<sub>3</sub> in the typical 26  
233 cities of the YRD in summer of 2018. O<sub>3</sub> concentration tended to be high in June, and relatively low



234 in July and August. The relatively low O<sub>3</sub> may be attributed to the maritime air masses transported  
235 by the Asian summer monsoon (Ding et al., 2008; Xu et al., 2008). Nevertheless, we notice that  
236 there are two regional multiday O<sub>3</sub> pollution episodes from 24 July to 11 August in the YRD, which  
237 means that about half of the cities in the YRD exceeded the national air quality standard (The national  
238 ambient air quality standard for MDA8 O<sub>3</sub> is 160 µg m<sup>-3</sup> in China). The first multiday O<sub>3</sub> episodes  
239 appeared in most cities from 24 July to 2 August. The highest MDA8 O<sub>3</sub> concentration reached up  
240 to 264 µg m<sup>-3</sup> on 27 July in Ningbo (NB). O<sub>3</sub> pollution was even observed for 6 consecutive days  
241 from 27 July to 1 August in Maanshan (MAS). Only two days later, regional O<sub>3</sub> pollution occurred  
242 in the YRD again from 5 August to 11 August.

243



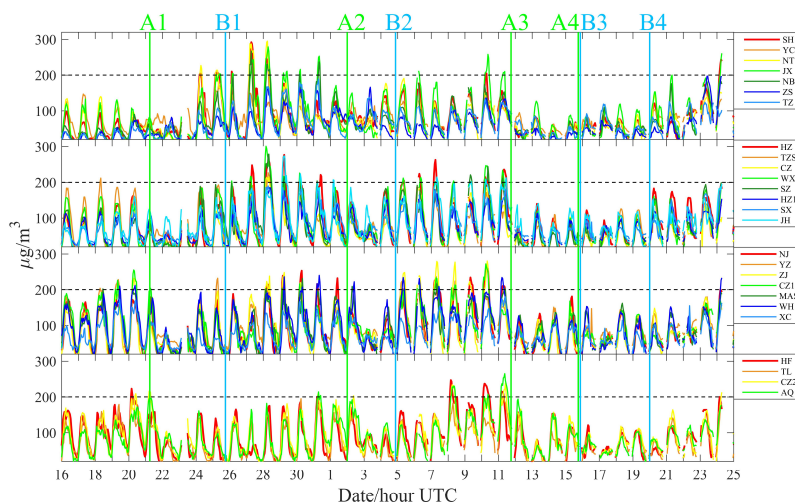
244  
245 **Figure 2. The MDA8 O<sub>3</sub> in 26 cities of the YRD in summer of 2018. The national ambient air**  
246 **quality standard for MDA8 O<sub>3</sub> is 160 µg m<sup>-3</sup> in China. These cities are sorted by longitude.**  
247

248 Figure 3 further shows diurnal variation of O<sub>3</sub> in all 26 cities of the YRD from 00:00 16 July  
249 to 00:00 25 August (throughout this paper the time refers to UTC, unless LST is specifically  
250 mentioned). Interestingly, O<sub>3</sub> pollution occurred earlier in cities near the coastline (large longitude,  
251 Figure 1b) rather than concurrently during the two multiday O<sub>3</sub> episodes. For example, from 24 July  
252 to 2 August, the first day that hourly O<sub>3</sub> concentration exceeded the national air quality standard  
253 (The national ambient air quality standard for hourly O<sub>3</sub> is 200 µg m<sup>-3</sup> in China) in Shanghai,  
254 Hangzhou, Nanjing and Hefei was 24 July, 27 July, 28 July and 31 July, respectively. Thus, we



255 classify the 26 cities in the YRD into four categories based on their longitudes, surrounding the four  
256 representative cities (Figure 4). The category I cities include SH, YC, NT, JX, NB, ZS and TZ. The  
257 category II cities include HZ, TZS, CZ, WX, SZ, HZ1, SX and JH, and the category III cities include  
258 NJ, YZ, ZJ, CZ1, MAS, WH and XC. Other cities are classified as the category IV cities, which are  
259 HF, TL, CZ2 and AQ. The first category cities are closest to the coastline, while the fourth category  
260 is the opposite.

261



262

263 **Figure 3. Diurnal variation of O<sub>3</sub> in all 26 cities of the YRD. The grey dotted lines are the**  
264 **national ambient air quality standard for hourly O<sub>3</sub> (200 µg m<sup>-3</sup>) in China. The letter A**  
265 **indicates the moment that the typhoon has reached the 24-h warning line, and letter B**  
266 **indicates the last moment of typhoon activity in the mainland China. These moments are**  
267 **acquired from the best-track TC dataset, depending on the start and end time of the densified**  
268 **observations. Coordinates 1, 2, 3, and 4 represent Typhoon Ampil, Typhoon Jongdari,**  
269 **Typhoon Yagi, and Typhoon Rumbia, respectively. Note: these cities are sorted by longitude.**

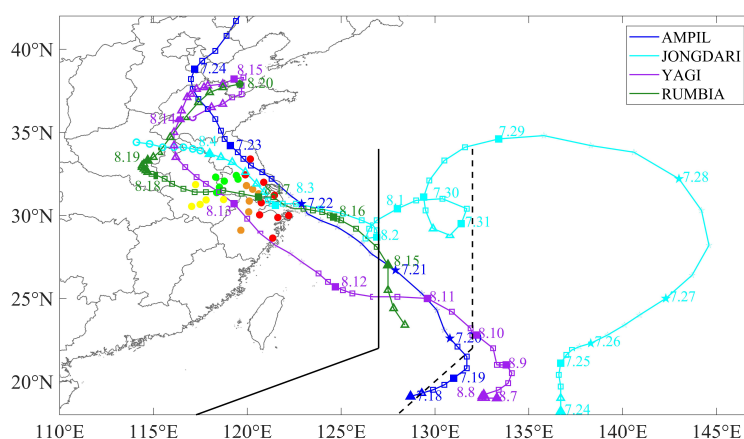
270

### 271 3.2 Landfall typhoons and their effects

272 For such O<sub>3</sub> episodes with regional, long-lasting characteristics, may often be associated with  
273 slow-moving synoptic weather systems. We find that the O<sub>3</sub> episodes coincided well with landfall  
274 typhoons activities, and the track and intensity of typhoons are given in Figure 4. Typhoon Ampil



275 was first observed at 00:00 on 18 July, and landed in Shanghai around 4:30 on 22 July with an  
276 intensity of severe tropical storm (IC=3). During the time of Typhoon Ampil, Typhoon Jongdari  
277 generated over the western North Pacific at 12:00 on 23 July, and made landfall at the junction of  
278 Zhejiang province and Shanghai at 21:00 1 August. After Typhoon Jongdari, Typhoon Yagi  
279 generated at 00:00 7 August. At around 15:35 12 August, it landed in Zhejiang province and  
280 remained active in the mainland China until 21:00 15 August. Before the end of Typhoon Yagi,  
281 Typhoon Rumbia was observed over the western North Pacific at 6:00 14 August. It finally landed  
282 in Shanghai at around 20:00 16 August, causing huge economic losses.  
283



284  
285 **Figure 4. The track and intensity of Typhoon Ampil, Typhoon Jongdari, Typhoon Yagi, and**  
286 **Typhoon Rumbia. The circle, triangle, square and pentagram indicate the intensity category**  
287 **of tropical cyclones is less than 1 (IC < 1), equal to 1 (IC = 1), equal to 2 (IC = 2), and not less**  
288 **than 3 (IC ≥ 3), respectively. Black solid line and dotted line represent the 24-hour and 48-h**  
289 **warning line for tropical cyclones, respectively. The colored solid points are the locations of**  
290 **cities in the YRD, and different color represents different cities categories. Wherein, red,**  
291 **carrot, green and yellow are category I, II, III and IV cities, respectively.**

292  
293 To further understand the relationship between O<sub>3</sub> episodes and landfall typhoons, we mark the  
294 critical moments of landfall typhoons in Figure 3. The letter A indicates the moment that typhoons  
295 have reached the 24-h warning line, and the letter B indicates the last moment of typhoon activity



296 in the mainland China. These moments are acquired from the best-track TC dataset, depending on  
297 the start and the end time of the densified observations. Coordinates 1, 2, 3, and 4 represent Typhoon  
298 Ampil, Typhoon Jongdari, Typhoon Yagi, and Typhoon Rumbia, respectively. As shown in Figure  
299 3, O<sub>3</sub> exhibited a significant cycle during the study period. That is, when the typhoon is close enough  
300 (near moments A1, A2, A3 and A4), the O<sub>3</sub> concentrations decreased, but O<sub>3</sub> concentrations would  
301 increase as long as the typhoon was not active in the mainland China (B1, B2 and B4) any more.  
302 This cycle would repeat if the next typhoon approached. O<sub>3</sub> pollution was likely to occur during the  
303 period from the end of the typhoon to the arrival of the next typhoon (B1A2 and B2A3) in the YRD.

304 Furthermore, we find that the variations of O<sub>3</sub> was related to the track, duration and landing  
305 intensity of the typhoons. For example, during the B1A2 period when the O<sub>3</sub> pollution occurred, the  
306 moments that hourly O<sub>3</sub> concentrations first exceed 200 µg m<sup>-3</sup> in about half of cities of the  
307 categories I, II, III and IV were 6:00 UTC (14:00 LST) 27 July, 6:00 UTC (14:00 LST) 28 July, 3:00  
308 UTC (11:00 LST) 29 July and 6:00 UTC (14:00 LST) 31 July, respectively. This phenomenon also  
309 suggests that O<sub>3</sub> pollution occurs in coastal region will be ahead of that in inland regions, which  
310 may be related to the track of typhoons (Figure 4). As for the impact of typhoon duration, the A4B3  
311 period provided a good interpretation. While Typhoon Yagi was still active in the mainland China,  
312 Typhoon Rumbia had reached the 24-hour warning line. Hence, the O<sub>3</sub> remained a low level  
313 throughout the period (A3B4), which was quite different from B1A2 and B2A3 period. Noted that  
314 the landing point and active path of Typhoon Ampil and Typhoon Jongdari were very similar (Figure  
315 4). However, the landing intensity of Typhoon Ampil was severe tropical storm (IC = 3), and that of  
316 Typhoon Jongdari was tropical storm (IC = 2), resulting in a difference in O<sub>3</sub> concentrations for  
317 Shanghai. Within 24 hours after Typhoon Ampil (Jongdari) reached the 24-hour warning line, the  
318 average O<sub>3</sub> concentrations was 40.9 (80.1) µg m<sup>-3</sup> in Shanghai. This is because that the stronger the  
319 typhoon landed, the gale (The 10-m wind speed near moment A1 was larger than that near moment  
320 A2 in Shanghai, Figure 7a) and precipitation accompanying the typhoon will be more effective in  
321 removing O<sub>3</sub>.

### 322 3.3 Processes of O<sub>3</sub> pollution affecting by typhoons

323 To reveal the major processes of O<sub>3</sub> pollution episodes affected by landfall typhoons, four  
324 representative cities (Shanghai, Hangzhou, Nanjing and Hefei) are selected for further analysis –  
325 based on monitoring data and model results.



### 3.3.1 Evaluation of model performance

To evaluate the simulation performance, the hourly simulation results are compared with the measurements during 00:00 16 July to 00:00 25 August. Table 3 presents the statistical metrics for selected variables, including temperature at 2 m ( $T_2$ ), relative humidity (RH), wind speed at 10 m ( $WS_{10}$ ) and wind direction at 10 m ( $WD_{10}$ ), and surface  $O_3$ .  $T_2$  is reasonably well simulated, with R values of 0.75, 0.77, 0.72 and 0.64 in Shanghai, Hangzhou, Nanjing and Hefei, respectively. Though our simulation underestimates  $T_2$  to some certain extent, the slightly underestimation is acceptable due to the small RMSE (3.2, 2.7, 2.9 and 3.3) and NMB (-7.5%, -5.1%, -5.5% and -5.5%) values. As for RH, the simulation results are overestimated in all four cities, leading to the NMB values of 9.1%, 4.6%, 6.7% and 0.5% in Shanghai, Hangzhou, Nanjing and Hefei, respectively. With high R values (0.69, 0.65, 0.71 and 0.71) and relatively low RMSE values (12.4, 12.8, 12.1 and 10.8), the WRF simulates RH over the YRD quite well. The wind fields are closely related to the transport processes of air pollutants. The overestimation of  $WS_{10}$  may partly be attributed to the unresolved terrain features by the default surface drag parameterization causing overestimation of wind speed in particular at low values (Jimenez and Dudhia, 2012; Li et al., 2017). With regards to  $WD_{10}$ , the simulation error is large based only on these statistical metrics. This is because that near-surface wind fields are deeply influenced by local underlying surface characteristics, and improving the urban canopy parameters might be useful (Liao et al., 2015; Xie et al., 2016). In term of  $O_3$ , the simulation results for  $O_3$  concentrations behave satisfactorily. R is as high as 0.55, 0.65, 0.66 and 0.54 in Shanghai, Hangzhou, Nanjing and Hefei, respectively, while the NMB values are 5.8%, 16.4%, -6.2% and -5.3%, respectively.

347

348 **Table 3. Statistical metrics for meteorological and chemical variables.**

City	Variable	$\bar{O}$	$\bar{S}$	R	RMSE	NMB
Shanghai	$T_2$ (°C)	30.3	28.1	0.75	3.2	-7.5%
	RH (%)	75.0	81.8	0.69	12.4	9.1%
	$WS_{10}$ ( $m s^{-1}$ )	4.9	5.5	0.51	2.3	11.7%
	$WD_{10}$ (°)	144.8	113.4	0.01	113.5	-22.9%
	$O_3$ ( $\mu g m^{-3}$ )	74.3	76.5	0.55	45.3	5.8%
Hangzhou	$T_2$ (°C)	30.3	28.8	0.77	2.7	-5.1%
	RH (%)	75.1	78.5	0.65	12.8	4.6%
	$WS_{10}$ ( $m s^{-1}$ )	3.3	4.7	0.32	2.7	32.5%



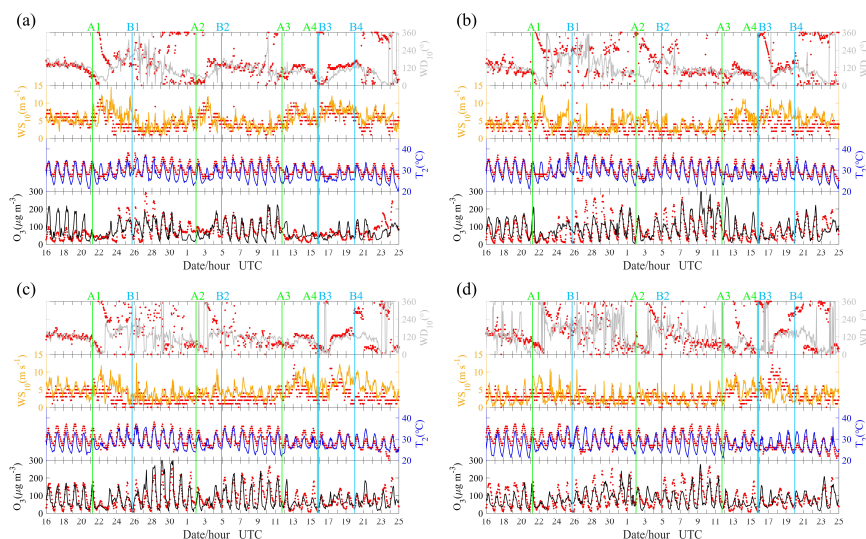
	WD <sub>10</sub> (°)	155.0	114.7	-0.10	132.5	-27.8%
	O <sub>3</sub> (μg m <sup>-3</sup> )	81.7	91.3	0.65	49.8	16.4%
Nanjing	T <sub>2</sub> (°C)	29.8	28.1	0.72	2.9	-5.5%
	RH (%)	77.4	82.6	0.71	12.1	6.7%
	WS <sub>10</sub> (m s <sup>-1</sup> )	3.1	5.0	0.39	3.0	63.8%
	WD <sub>10</sub> (°)	132.8	115.6	0.21	102.7	-15.0%
	O <sub>3</sub> (μg m <sup>-3</sup> )	87.6	79.8	0.66	46.7	-6.2%
Hefei	T <sub>2</sub> (°C)	29.3	27.7	0.64	3.3	-5.5%
	RH (%)	81.1	81.5	0.71	10.8	0.5%
	WS <sub>10</sub> (m s <sup>-1</sup> )	3.2	3.2	0.37	2.2	2.9%
	WD <sub>10</sub> (°)	147.0	128.6	0.04	136.7	-13.3%
	O <sub>3</sub> (μg m <sup>-3</sup> )	87.3	80.3	0.54	45.0	-5.3%

349 Note. R exceeds 0.1 to reach statistically significant at 99.9% confident level.

350

351 Figure 5 further shows hourly variations of O<sub>3</sub>, T<sub>2</sub>, WS<sub>10</sub> and WD<sub>10</sub> for measurements and  
 352 simulations in four representative cities. The simulations effectively reproduce the diurnal variation  
 353 of O<sub>3</sub>, T<sub>2</sub> and WS<sub>10</sub>, confirming the reliability of the simulation results. Moreover, the model well  
 354 captures the shift in wind direction during the study period. Thus, the overall model performance  
 355 for wind fields is acceptable. In summary, the simulation results can capture and reproduce the major  
 356 characteristics of the O<sub>3</sub> episodes, including the meteorological conditions and evolution of O<sub>3</sub>,  
 357 which can provide valuable insights into the formation of the O<sub>3</sub> episodes.

358



359

360



361 **Figure 5. Hourly variations of O<sub>3</sub>, T<sub>2</sub>, WS<sub>10</sub> and WD<sub>10</sub> for measurements (red dots) and**  
362 **simulation (colored lines) in (a) Shanghai, (b) Hangzhou, (c) Nanjing and (d) Hefei.**

363

### 364 3.3.2 Shanghai in category I cities

365 In this study, Shanghai was usually one of the first cities affected by landfall typhoons. We can  
366 see a multiday episode of O<sub>3</sub> during the period of 24–28 July, with a maximum of hourly O<sub>3</sub> up to  
367 292 μg m<sup>-3</sup> at 27 July (Figure 6a). The high O<sub>3</sub> concentrations together with high primary pollutants  
368 (CO and NO<sub>2</sub>) suggest a strong photochemical O<sub>3</sub> production under the condition of high  
369 temperature (The daily maximum temperature can reach 35 °C) during this period, and the weak  
370 wind may play a significant role in the accumulation of surface O<sub>3</sub>. The increase of primary  
371 pollutants may be related to the wind shift from southeast to southwest causing by Typhoon Ampil  
372 (A1 in Figure 6a, -A1 and A1B1 in Figure 7), resulting in air masses originally from the ocean had  
373 become inland. Interestingly, PM<sub>2.5</sub> also showed good correlation with O<sub>3</sub> and primary pollutants,  
374 especially for NO<sub>2</sub> during this period. This indicates that a high level of oxidizability can promote  
375 the formation of secondary particles (Kamens et al., 1999; Khoder, 2002). From the results of  
376 process analysis (Figure 6b), the major contributions to surface O<sub>3</sub> were TDIF, CHEM and DDEP  
377 due to the small net contribution of MADV. TDIF had a considerable positive contribution while  
378 DDEP did the opposite, suggesting that high surface O<sub>3</sub> may be sourced from the upper layer via  
379 TDIF process, and be removed via DDEP process. However, for the whole boundary layer, which  
380 is defined as the layer less than 1500 m in this study, it was the balance between CHEM and DDEP  
381 instead TDIF and DDEP. Thus, TDIF was likely to play the role of “transport” from the upper layer  
382 to surface. Figure 6c further shows the temporal-vertical distribution of O<sub>3</sub> with vertical wind  
383 velocity. The downward airflows were prevailed over Shanghai until 23 July, which are induced by  
384 the subtropical high. Then, strong upward airflows appeared as Typhoon Ampil arrived, and high  
385 level of O<sub>3</sub> disappeared. Around 27 July, the downward airflows gradually resumed and high level  
386 of O<sub>3</sub> occurred. It is note-worthy that the high value center of O<sub>3</sub> appeared near the altitude of 1 km  
387 instead of near surface, indicting high photochemical production efficiency of O<sub>3</sub> occurred in the  
388 middle boundary layer. The downward airflows can not only inhibit the vertical transport of O<sub>3</sub> but  
389 also transport high-level O<sub>3</sub> to the surface, causing the episodes of surface O<sub>3</sub>.

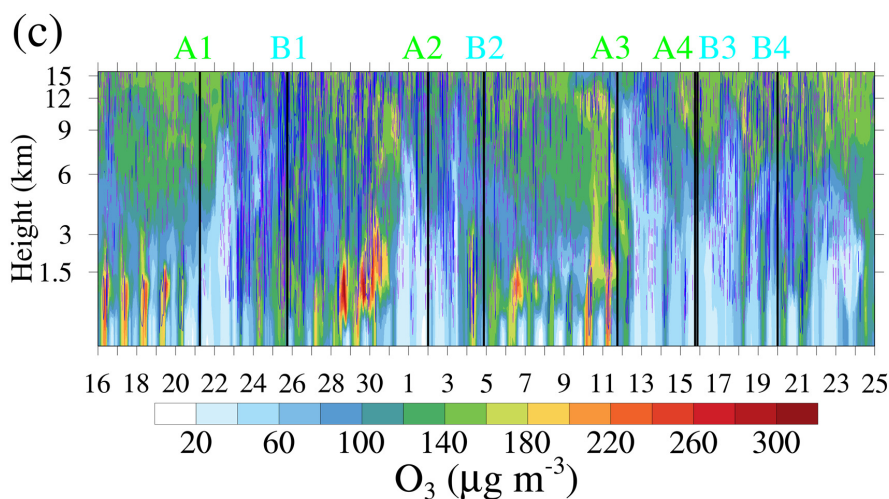
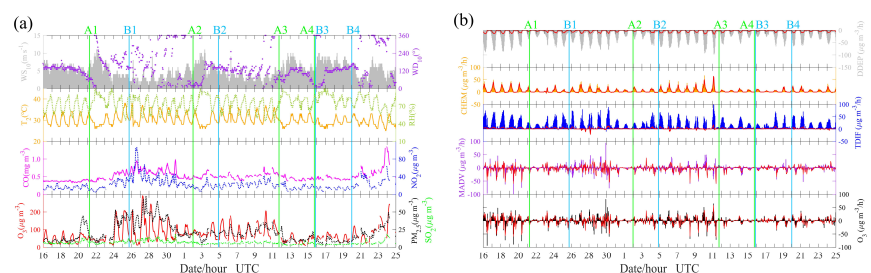
390 As shown in Figure 7, O<sub>3</sub> pollution tends to occur during the period from the end of the typhoon



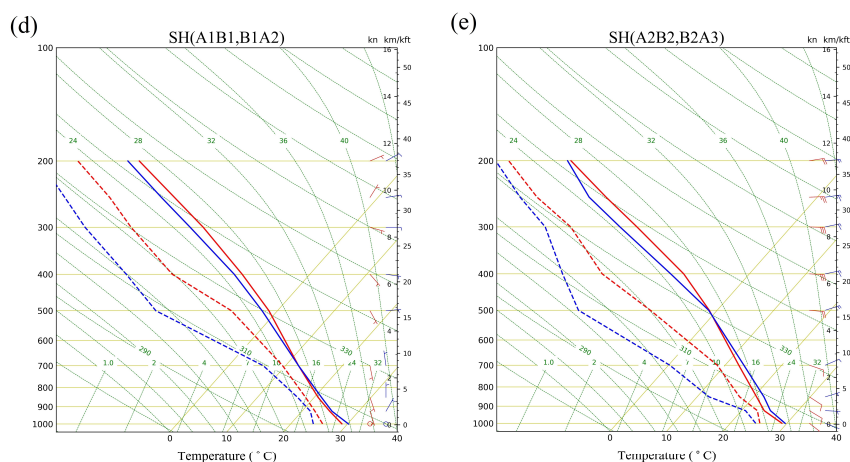
391 to the arrival of the next typhoon (B1A2 and B2A3) in the YRD. To reveal this phenomenon, we  
 392 compare these two periods (B1A2 and B2A3) with their previous periods (A1B1 and A2B2) using  
 393 the skew-T log-P diagram (Figure 6d and 6e). It is found that the atmospheric conditions of B1A2  
 394 (B2A3) were hotter and drier than A1B1 (A2B2) below 700 hPa in Shanghai, and wind speed is  
 395 smaller in B1A2 (B2A3). Those changes in atmospheric conditions after typhoon will be conducive  
 396 to the generation of high O<sub>3</sub> concentration in Shanghai.

397

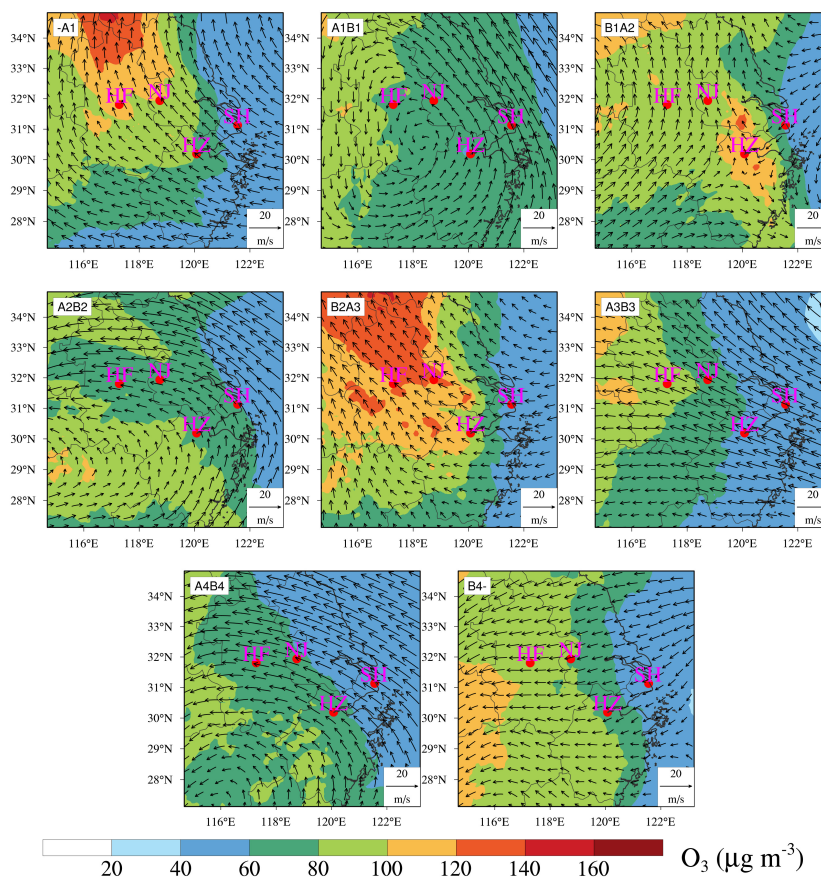
398



399



400  
401 **Figure 6. (a) Time series of air pollutants ( $O_3$ ,  $PM_{2.5}$ ,  $SO_2$ ,  $CO$  and  $NO_2$ ) and meteorological**  
402 **factors ( $T_2$ ,  $RH$ ,  $WS_{10}$  and  $WD_{10}$ ) in Shanghai. (b) Individual processes contribution to net  $O_3$**   
403 **density at Shanghai.  $O_3$  is the net increase,  $MADV$  is the sum of horizontal advection ( $HADV$ )**  
404 **and vertical advection ( $ZADV$ ),  $TDIF$  is the sum of horizontal diffusion ( $HDIF$ ) and vertical**  
405 **diffusion ( $VDIF$ ),  $CHEM$  is chemical reaction process, and  $DDEP$  is dry deposition process.**  
406 **The color histograms indicate the results for the layer near the surface, while the solid red**  
407 **lines indicate the average results for all layers below 1500 m. (c) Temporal-vertical distribution**  
408 **of  $O_3$  with vertical wind velocity over Shanghai. The dotted purple line and solid blue line**  
409 **indicate the negative wind speeds (downward airflows) and positive wind speeds (upward**  
410 **airflows), respectively. (d) The skew-T log-P diagram at Shanghai. The average results of**  
411 **period A1B1 and B1A2 are shown in red and blue, respectively. (e) Same as (d), but for the**  
412 **average results of period A2B2 and B2A3.**  
413



414  
415 **Figure 7.** Spatial distribution of surface O<sub>3</sub> with wind fields at 850 hPa over the YRD. -A1,  
416 A1B1, B1A2, A2B2, B2A3, A3B3, A4B4, B4- are the average results from the beginning to A1,  
417 A1 to B1, B1 to A2, A2 to B2, B2 to A3, A3 to B3, A4 to B4, B4 to the end, respectively. Details  
418 can be found in Figure 4.

419

### 420 3.3.3 Hangzhou in category II cities

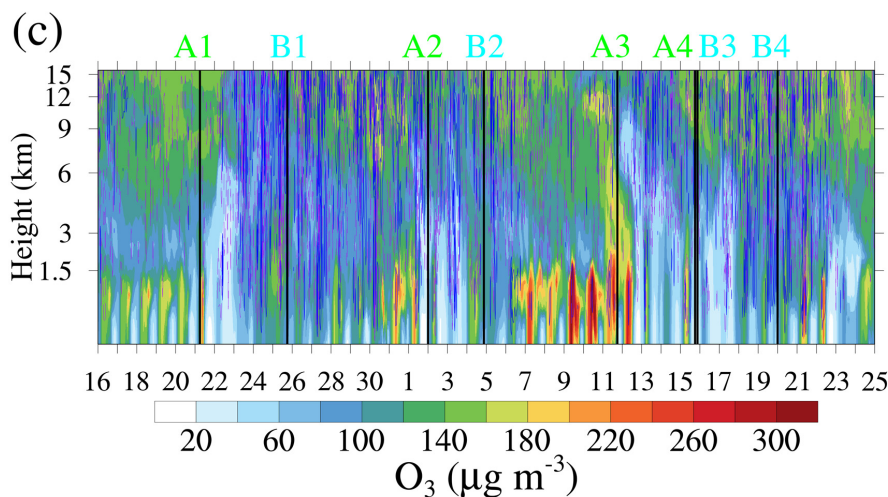
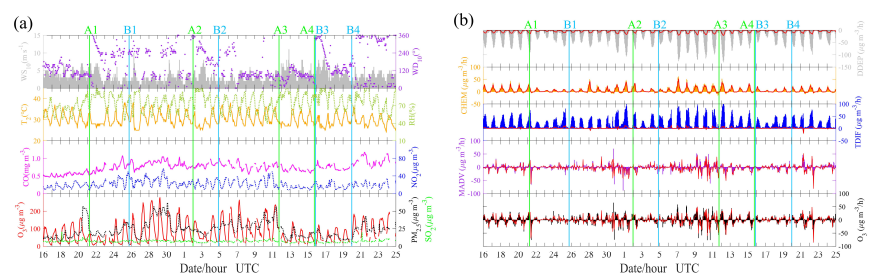
421 Figure 8 presents the results for Hangzhou. It shows that high O<sub>3</sub> concentrations occurred on  
422 27-31 July and 5-7 August, which may also be related to the strong photochemical production of O<sub>3</sub>  
423 under the abundance of precursors (Figure 8a) and poor diffusion conditions due to the light wind  
424 (B1A2 and B2A3 in Figure 7). Figure 8a further shows that high O<sub>3</sub> was often associated with an  
425 increase in CO but the NO<sub>2</sub> concentrations usually remained at the same level. This phenomenon  
426 indicates a VOCs-limited regime in this city since CO usually have good correlation with VOCs



427 and can play a similar role as VOCs in the photochemical production of O<sub>3</sub> (Atkinson, 2000; Ding  
428 et al., 2013). In fact, O<sub>3</sub> in other representative cities (Shanghai, Nanjing and Hefei) also showed a  
429 better correlation with CO than NO<sub>2</sub>. Though Hangzhou is close to Shanghai, there is a significant  
430 difference of wind fields over these two cities. Starting from the arrival of Typhoon Ampil (A1).  
431 The wind direction in Hangzhou did not change back to southeast until a few days later after  
432 Typhoon Jongdari dissipated (B2). During this period (A1B2), the frequent southwest wind may be  
433 the reason for high CO concentrations in Hangzhou. In addition, the chaotic wind field during period  
434 B1A2 (B1A2 in Figure 7) may lead to the light wind in Hangzhou. With respect to the simulation  
435 results, the model simulated the variation of O<sub>3</sub> but failed to capture the O<sub>3</sub> peaks (e.g., the peak  
436 values on 27–31 July), which may be related to the strong upward airflows (Figure 8c) that inhibited  
437 the accumulation of O<sub>3</sub> (Figure 8b). This further illustrates that downward airflows may be an  
438 important factor for O<sub>3</sub> episodes in this case.

439

440



441



442 **Figure 8. Same as Figure 6 (a)-(c), but for Hangzhou.**

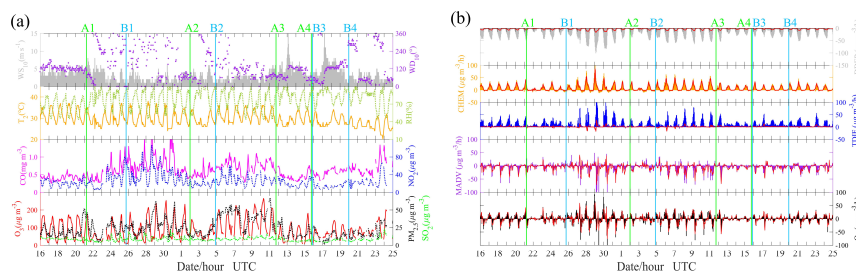
443

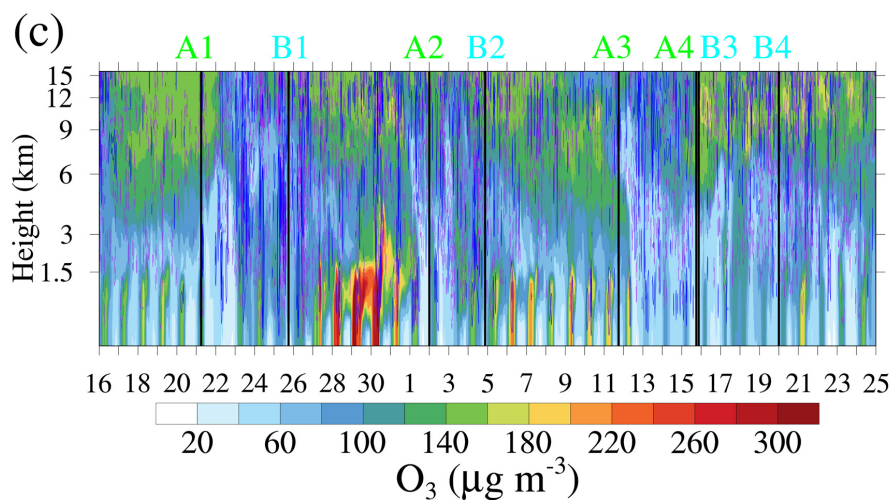
### 444 3.3.4 Nanjing in category III cities

445 As for Nanjing, the O<sub>3</sub> episodes with exceedance of national air quality standards were  
446 observed on 28 July to 1 August and 7-11 August. These O<sub>3</sub> episodes were characterized by abundant  
447 O<sub>3</sub> precursors under the condition of high temperature. Furthermore, light wind (B1A2 and B2A3  
448 in Figure 7) and downward airflows (Figure 9c) also contributed greatly to the occurrence of O<sub>3</sub>  
449 pollution, with the similar mechanism as that of Shanghai and Hangzhou. As early as 22 July, the  
450 wind direction in Nanjing had changed from southeast to southwest affected by Typhoon Ampil,  
451 and the concentrations of the main primary pollutants (CO, NO<sub>2</sub> and SO<sub>2</sub>) increased (Figure 9a).  
452 However, high-level O<sub>3</sub> episodes did not occur until 28 July even though the maximum temperature  
453 did not change significantly during 24-31 July. The “obstacle” of the O<sub>3</sub> episodes may be the  
454 precipitation causing by the strong upward airflows during 23-26 July (Figure 9c). As shown in  
455 Figure 9b, high surface O<sub>3</sub> concentration during the pollution episodes is the result of TDIF and  
456 CHEM processes, and is lost through DDEP and MADV processes. With respect to the vertical  
457 structure of atmospheric, B1A2 (B2A3) was also hotter and drier than A1B1 (A2B2) below 700 hPa  
458 in Nanjing (Figure 9d and 9e). The similar results as Shanghai further confirm that high O<sub>3</sub>  
459 concentrations are more likely to occur during the period from the end of the typhoon to the arrival  
460 of the next typhoon (B1A2 and B2A3) than the period when the typhoon approaches and is active  
461 in the mainland China (A1B1 and A2B2).

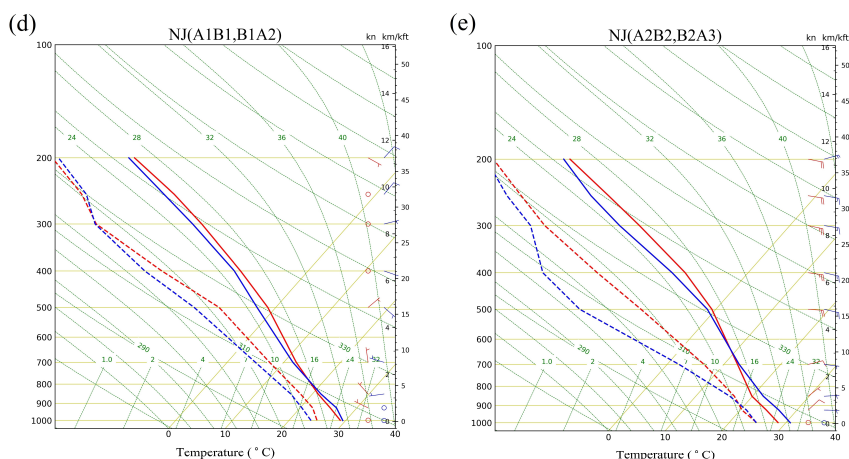
462

463





464



465

466 **Figure 9.** Same as Figure 6, but for Nanjing.

467

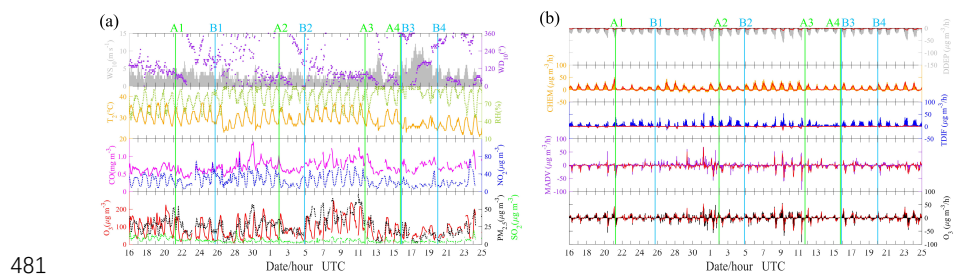
### 468 3.3.5 Hefei in category IV cities

469 Hefei is the city farthest from the coast among four representative cities, and O<sub>3</sub> pollution  
470 occurred on 31 July and 8-11 August. We can also find the phenomenon that the precursors  
471 concentrations had an increase once the wind direction changed from southeast to southwest (Figure  
472 10a). During B1A2 and B2A3, the main precursors of O<sub>3</sub> had a high level. However, high O<sub>3</sub>  
473 concentration was mainly found in B2A3, and not in B1A2. This may be related to the relatively  
474 low temperature during B1A2 (Figure 10a), which is not conducive to photochemical production of

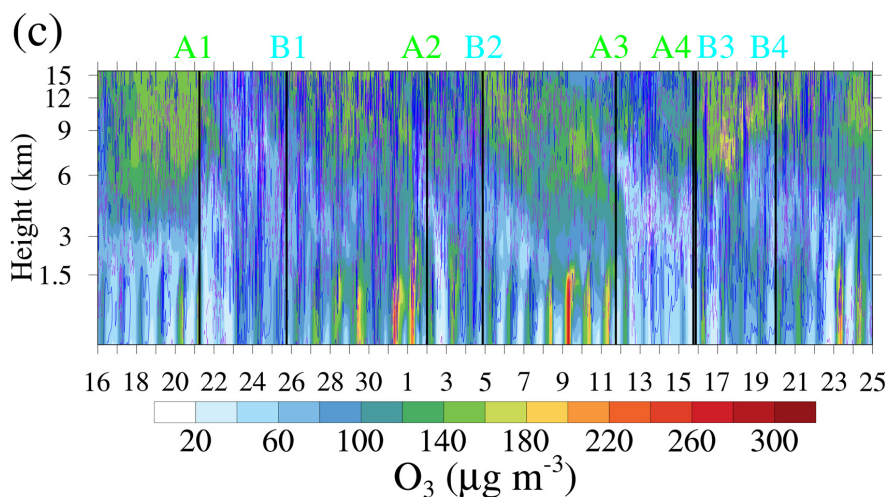


475 O<sub>3</sub> (Figure 10b). As shown in Figure 10c, there were distinct upward airflows within the boundary  
476 layer, which may be related to urban effect (e.g., urban heat islands). These upward airflows within  
477 the boundary layer help mix the air, resulting in a uniform distribution of O<sub>3</sub> in the vertical direction.  
478 However, the downward airflows can still inhibit the vertical diffusion of O<sub>3</sub>, and O<sub>3</sub> tends to be  
479 trapped within the boundary layer.

480



481



482

483 **Figure 10.** Same as Figure 6 (a)-(c), but for Hefei.

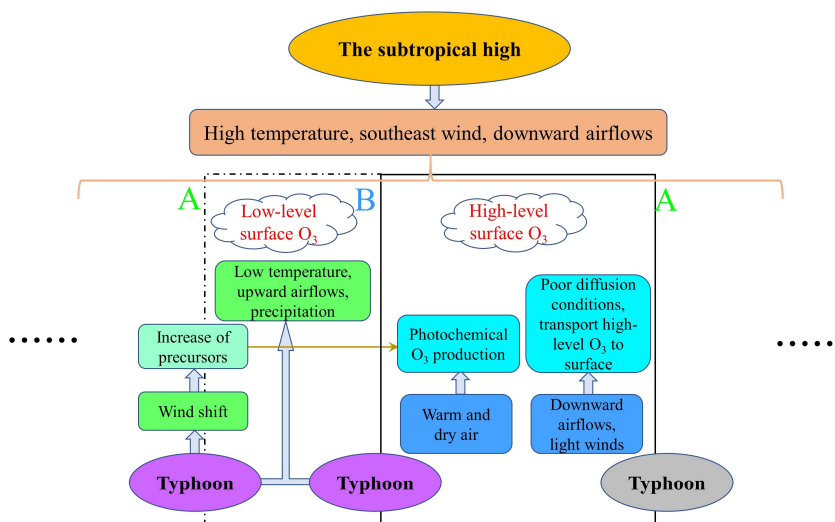
484

### 485 3.3.6 A schematic diagram of major processes

486 Although the processes of landfall typhoon affecting O<sub>3</sub> varied from city to city, the major  
487 processes have many similarities and can be summarized as a schematic diagram in Figure 11. The  
488 YRD region, which features a typical subtropical monsoon climate, is strongly influenced by the  
489 western Pacific subtropical high in summer. Dominated by the subtropical high, the meteorological



490 conditions of high temperature and downward airflows combined with high levels of precursors due  
491 to the huge energy consumption tend to form high O<sub>3</sub> concentrations in this region. However,  
492 powerful systems like typhoon can break this state. For typhoons that may land in the YRD, by the  
493 time they approach the 24-hour warning line, the prevailing southeast wind in the YRD will change  
494 to southwest wind, which can transport lots of precursors from inland to the YRD. The change in  
495 wind direction depends on the track of typhoon and the geographical location of cities, and often  
496 appears first in coastal region. With typhoon, the low temperature, precipitation (upward airflows)  
497 and wild wind will prevent high O<sub>3</sub> and PM<sub>2.5</sub> episodes. Moreover, the effect of removing pollutants  
498 is related to the intensity of typhoon landing, but some of the main precursors of O<sub>3</sub> are still at a  
499 high level due to foreign sources superposed with local emissions. After typhoon, the atmosphere  
500 returns to a warm and dry state (even more so than before), and strong photochemical reactions  
501 begin to produce O<sub>3</sub> under the abundance of precursors. O<sub>3</sub> is mainly generated inside the boundary  
502 layer (~1000 m), and then transported to the surface by downward airflows or turbulent mixing. At  
503 the same time, the wind readjusts to southeast and wind speed is light, resulting in poor diffusion  
504 conditions. The downward airflows and light wind obstruct the vertical and horizontal diffusion of  
505 O<sub>3</sub>, leaving O<sub>3</sub> trapped on the ground. The thermal-dynamic effects result in high-level surface O<sub>3</sub>  
506 in the YRD.  
507



508



509 **Figure 11. A schematic diagram of major processes that summertime O<sub>3</sub> affected by landfall**  
510 **typhoon in the YRD. The letter A indicates the moment that the typhoon has reached the 24-**  
511 **h warning line, and letter B indicates the last moment of typhoon activity in the mainland**  
512 **China.**

513

514 In fact, most typhoons generated over the western North Pacific will not land in China, or they  
515 are more likely to land in the South China rather than the YRD. In our previous study (Shu et al.,  
516 2016), the typhoon did not land in the YRD, but the processes of high-level O<sub>3</sub> formation may be  
517 common. That is, the processes in the dashed box in Figure 11 are unique to landfall typhoons, while  
518 the processes in the solid box can be found as long as the typhoons that can affect the YRD.  
519 Transport of precursors, downward airflows, high temperature and light wind are crucial factors,  
520 and the roles of those factors play in O<sub>3</sub> episodes depends on typhoon and city. It is hard to quantify  
521 these processes with just a few cases. For example, we cannot estimate whether the downward  
522 airflows are dominated by the subtropical high or the periphery circulation of typhoons since they  
523 usually occur simultaneously. Furthermore, the behave of particulate matter is intriguing since high-  
524 level PM<sub>2.5</sub> often occurs with high-level O<sub>3</sub> after typhoon, which is different from previous studies  
525 that high particulate matter concentrations inhibit the formation of O<sub>3</sub> (Li et al., 2005; Xing et al.,  
526 2017). This may be related to the heterogeneous reactions (Lou et al., 2014) but research on this  
527 issue is quite limited to date.

528

### 529 **3.3 Premature mortalities induced by O<sub>3</sub> exposure**

530 When it comes to typhoons, especially landfall typhoons, the first concern is the huge damage  
531 caused by extreme weathers. After typhoons, people are relieved and busy with their work as usual.  
532 However, our research indicates that high O<sub>3</sub> episodes are likely to occur in the short period after a  
533 typhoon in the YRD, and high O<sub>3</sub> concentrations can do harm to people's health. To arouse attention  
534 on this issue, we estimate the premature mortality attributed to O<sub>3</sub> for respiratory disease, we choose  
535 two complete cycles, which is the period A1A3 (21 July to 11 August), to do the calculation. Table  
536 4 summarized the premature mortalities in cities in the YRD. The premature mortalities are a  
537 function of both the population and O<sub>3</sub> levels, resulting in high premature mortalities in populated  
538 and heavily polluted areas. Out of the 26 cities in the YRD, Shanghai shows highest premature



539 mortalities (29.2) due to its high surface O<sub>3</sub> concentrations and huge population. The city with the  
540 lowest premature mortalities (0.6) is Zhoushan, which may be related to removing effect of the  
541 maritime air masses as Zhoushan is located by the sea (Figure 1b). During this period, the total  
542 premature mortalities in the YRD is 194.0, which is larger than the number of casualties caused  
543 directly by the typhoons (80 people were killed by landfall typhoons in mainland China in 2018).

544

545 **Table 4. Premature mortalities induced by O<sub>3</sub> exposure for respiratory disease**

	City	Population (thousand)	Premature mortalities
Category I cities	Shanghai	24,240	29.2
	Yancheng	7,200	6.1
	Nantong	7,310	7.9
	Jiaxing	4,726	7.3
	Ningbo	8,202	8.1
	Zhoushan	1,173	0.6
	Taizhou	6,139	4.1
Category II cities	Hangzhou	9,806	16.5
	Taizhoushi	4,636	5.2
	Changzhou	4,729	4.4
	Wuxi	6,575	10.7
	Suzhou	10,722	15.3
	Huzhou	3,027	2.8
	Shaoxing	5,035	4.7
	Jinhua	5,604	8.2
Category III cities	Nanjing	8,436	13.4
	Yangzhou	4,531	5.5
	Zhenjiang	3,196	5.3
	Chuzhou	4,114	5.8
	Maanshan	2,337	3.6
	Wuhu	3,748	6.2
	Xuancheng	2,648	2.0
Category IV cities	Hefei	8,087	10.9
	Tongling	1,629	1.7
	Chizhou	1,475	2.1
	Anqing	4,691	6.4
Total		154,016	194.0

546

547 **4 Conclusions**



548 In this study, we investigate the detail processes of landfall typhoons affecting O<sub>3</sub> in the YRD  
549 based on a unique case during 16 July to 25 August with the help of monitoring observations and  
550 numerical simulations. This case was characterized by two multiday regional O<sub>3</sub> pollution episodes  
551 concerned with four successive landfall typhoons. The two O<sub>3</sub> episodes appeared from 24 July to 2  
552 August and 5 to 11 August, respectively, with the highest MDA8 O<sub>3</sub> reached up to 264 μg m<sup>-3</sup>.

553 The moment that typhoon reaches the 24-h warning line and the last moment of typhoon  
554 activity in the mainland China are crucial, because O<sub>3</sub> pollution episodes mainly occurred during  
555 the period from the end of typhoon and the arrival of the next typhoon in the YRD. These two  
556 moments can be roughly regarded as time nodes. Furthermore, it is found that the variations of O<sub>3</sub>  
557 was related to the track, duration and landing intensity of the typhoons during the study period. O<sub>3</sub>  
558 pollution appeared in coastal region was ahead of that in inland regions due to the track of typhoons.  
559 The interval between two typhoons can affect the duration of high O<sub>3</sub> concentration in the YRD.  
560 Generally, sustained high O<sub>3</sub> concentration tends to appear on days when the typhoon has dissipated  
561 but not influenced by the new one. As for the landing intensity of typhoon, the stronger the typhoon  
562 landed, the gale and precipitation accompanying the typhoon will be more effective in removing O<sub>3</sub>,  
563 resulting in lower O<sub>3</sub> concentration in the typhoon landing location.

564 The detail processes of landfall typhoons affecting O<sub>3</sub> depend on typhoons and cities. High  
565 temperature and downward airflows dominated by the subtropical high combined with abundant  
566 precursors are the main reason for high O<sub>3</sub> concentration in the YRD in summer. And landfall  
567 typhoon can change this state through the following mechanism: When the landfall typhoon is close  
568 enough (~ 24-hour warning line), the prevailing southeast wind will change to southwest wind,  
569 which transports large amount of precursors from inland to the YRD. The southwest wind usually  
570 appears first in coastal region, and will turn back to southeast wind as long as the YRD is dominated  
571 by subtropical high. Then the typhoon makes landfall, the low temperature, precipitation (upward  
572 airflows) and wild wind suppress the generation of O<sub>3</sub>. After typhoon, the atmosphere at low layer  
573 (below 700 hPa) will be warm and dry, and strong photochemical reactions begin to produce O<sub>3</sub>  
574 under the abundance of precursors due to foreign sources superposed with local emissions. O<sub>3</sub> is  
575 mainly generated in the middle of boundary layer (~ 1000 m), and then transported to the surface  
576 by downward airflows or turbulent mixing. The downward airflows also obstruct the vertical  
577 diffusion of O<sub>3</sub>. Meanwhile, wind speed is light when the wind readjusts to southeast, which further



578 worsens horizontal diffusion of O<sub>3</sub>. The O<sub>3</sub> can be accumulated and trapped on the ground. The  
579 thermal-dynamic effects results in high surface O<sub>3</sub> concentration in the YRD. Those processes will  
580 repeat if the next typhoon approach.

581 The estimated premature mortalities attributed to O<sub>3</sub> exposure for respiratory disease in the  
582 YRD during 21 July to 11 August (two complete cycles of typhoons) is 194.0, which is larger than  
583 the number of casualties caused directly by the typhoons. This work can enhance our understanding  
584 of how landfall typhoons affect O<sub>3</sub> in the YRD, which may help to forecast the O<sub>3</sub> pollution  
585 synthetically impacted by the subtropical high and typhoon. Meanwhile, our results further confirm  
586 that large-scale synoptic weather systems play an important role in regional air pollution, suggesting  
587 a need in establishing potential links between air pollution and predominant synoptic patterns.

588

589 **Author contributions.** C. C. Zhan and M. Xie had the original ideas, designed the research, collected  
590 the data, and prepared the original draft. C. C. Zhan carried out the data analysis. M. Xie acquired  
591 financial support for the project leading to this publication. C. W. Huang taught and helped C. C.  
592 Zhan to do the numerical simulation. T. J. Wang and J. Liu revised the manuscript and helped to  
593 collect the data. C. Q. Ma helped to deal with the emission inventory. M. Xu and J. W. Yu helped to  
594 collect the data. M. M. Li, S. Li, B. L. Zhuang, and M. Zhao reviewed the initial draft and checked  
595 the English of the original manuscript. Y. M. Jiao and D. Y. Nie reviewed the initial draft and helped  
596 to improve the work of health impact.

597

598 **Acknowledgements.**

599 This work was supported by the National Key Research and Development Program of China  
600 (2018YFC0213502, 2018YFC1506404), the open research fund of Chongqing Meteorological  
601 Bureau (KFJJ-201607) and the Fundamental Research Funds for the Central Universities  
602 (020714380047).

603

604 **References**

605 Allen, R. J., Sherwood, S. C., Norris, J. R., and Zender, C. S.: Recent Northern Hemisphere tropical  
606 expansion primarily driven by black carbon and tropospheric ozone, *Nature*, 485, 350-354,  
607 10.1038/nature11097, 2012.



- 608 Anenberg, S. C., Horowitz, L. W., Tong, D. Q., and West, J. J.: An estimate of the global burden of  
609 anthropogenic ozone and fine particulate matter on premature human mortality using  
610 atmospheric modeling, *Environ Health Perspect*, 118, 1189-1195, 10.1289/ehp.0901220, 2010.
- 611 Burnett, R. T., Pope, C. A., 3rd, Ezzati, M., Olives, C., Lim, S. S., Mehta, S., Shin, H. H., Singh, G.,  
612 Hubbell, B., Brauer, M., Anderson, H. R., Smith, K. R., Balmes, J. R., Bruce, N. G., Kan, H.,  
613 Laden, F., Pruss-Ustun, A., Turner, M. C., Gapstur, S. M., Diver, W. R., and Cohen, A.: An  
614 integrated risk function for estimating the global burden of disease attributable to ambient fine  
615 particulate matter exposure, *Environ Health Perspect*, 122, 397-403, 10.1289/ehp.1307049,  
616 2014.
- 617 Chameides, W., and Walker, J. C. G.: A photochemical theory of tropospheric ozone, *Journal of*  
618 *Geophysical Research*, 78, 8751-8760, 10.1029/JC078i036p08751, 1973.
- 619 Chan, C. K., and Yao, X.: Air pollution in mega cities in China, *Atmospheric Environment*, 42, 1-  
620 42, 10.1016/j.atmosenv.2007.09.003, 2008.
- 621 Deng, T., Wang, T., Wang, S., Zou, Y., Yin, C., Li, F., Liu, L., Wang, N., Song, L., Wu, C., and Wu,  
622 D.: Impact of typhoon periphery on high ozone and high aerosol pollution in the Pearl River  
623 Delta region, *The Science of the total environment*, 668, 617-630,  
624 10.1016/j.scitotenv.2019.02.450, 2019.
- 625 Ding, A. J., Wang, T., Thouret, V., Cammas, J. P., and Nedelec, P.: Tropospheric ozone climatology  
626 over Beijing: analysis of aircraft data from the MOZAIC program, *Atmospheric Chemistry and*  
627 *Physics*, 8, 1-13, 2008.
- 628 Ding, A. J., Fu, C. B., Yang, X. Q., Sun, J. N., Zheng, L. F., Xie, Y. N., Herrmann, E., Nie, W., Petäjä,  
629 T., Kerminen, V. M., and Kulmala, M.: Ozone and fine particle in the western Yangtze River  
630 Delta: an overview of 1 yr data at the SORPES station, *Atmospheric Chemistry and Physics*,  
631 13, 5813-5830, 10.5194/acp-13-5813-2013, 2013.
- 632 Ding, A., Nie, W., Huang, X., Chi, X., Sun, J., Kerminen, V.-M., Xu, Z., Guo, W., Petäjä, T., Yang,  
633 X., Kulmala, M., and Fu, C.: Long-term observation of air pollution-weather/climate  
634 interactions at the SORPES station: a review and outlook, *Frontiers of Environmental Science*  
635 *& Engineering*, 10, 10.1007/s11783-016-0877-3, 2016.
- 636 Dong J Y, Liu X R, Zhang B Z.: Meta-analysis of association between short-term ozone exposure  
637 and population mortality in China, *Acta Scientiae Circumstantiae*, 36 (4), 1477-1485, 2016 (in



- 638 Chinese).
- 639 Fan, Q., Lan, J., Liu, Y. M., Wang, X. M., Chan, P. W., Hong, Y. Y., Feng, Y. R., Liu, Y. X., Zeng, Y.  
640 J., and Liang, G. X.: Process analysis of regional aerosol pollution during spring in the Pearl  
641 River Delta region, China, *Atmospheric Environment*, 122, 829-838, 2015.
- 642 Ghude, S. D., Chate, D. M., Jena, C., Beig, G., Kumar, R., Barth, M. C., Pfister, G. G., Fadnavis, S.,  
643 and Pithani, P.: Premature mortality in India due to PM<sub>2.5</sub> and ozone exposure, *Geophys Res*  
644 *Lett*, 43, 4650-4658, 10.1002/2016gl068949, 2016.
- 645 Guo, S., Hu, M., Zamora, M. L., Peng, J., Shang, D., Zheng, J., Du, Z., Wu, Z., Shao, M., Zeng, L.,  
646 Molina, M. J., and Zhang, R.: Elucidating severe urban haze formation in China, *Proceedings*  
647 *of the National Academy of Sciences of the United States of America*, 111, 17373-17378,  
648 10.1073/pnas.1419604111, 2014.
- 649 Hu, J., Chen, J., Ying, Q., and Zhang, H.: One-year simulation of ozone and particulate matter in  
650 China using WRF/CMAQ modeling system, *Atmospheric Chemistry and Physics*, 16, 10333-  
651 10350, 10.5194/acp-16-10333-2016, 2016.
- 652 Huang, J.-P.: Numerical simulation and process analysis of typhoon-related ozone episodes in Hong  
653 Kong, *Journal of Geophysical Research*, 110, 10.1029/2004jd004914, 2005.
- 654 Huang, R. J., Zhang, Y., Bozzetti, C., Ho, K. F., Cao, J. J., Han, Y., Daellenbach, K. R., Slowik, J.  
655 G., Platt, S. M., Canonaco, F., Zotter, P., Wolf, R., Pieber, S. M., Bruns, E. A., Crippa, M.,  
656 Ciarelli, G., Piazzalunga, A., Schwikowski, M., Abbaszade, G., Schnelle-Kreis, J.,  
657 Zimmermann, R., An, Z., Szidat, S., Baltensperger, U., El Haddad, I., and Prevot, A. S.: High  
658 secondary aerosol contribution to particulate pollution during haze events in China, *Nature*,  
659 514, 218-222, 10.1038/nature13774, 2014.
- 660 Jerrett, M., Burnett, R. T., Pope, C. A., Ito, K., Thurston, G., Krewski, D., Shi, Y. L., Calle, E., and  
661 Thun, M.: Long-Term Ozone Exposure and Mortality., *New Engl J Med*, 360, 1085-1095, 2009.
- 662 Jiménez, P. A., and Dudhia, J.: Improving the Representation of Resolved and Unresolved  
663 Topographic Effects on Surface Wind in the WRF Model, *Journal of Applied Meteorology and*  
664 *Climatology*, 51, 300-316, 10.1175/jamc-d-11-084.1, 2012.
- 665 Jin, Y., Andersson, H., and Zhang, S.: Air Pollution Control Policies in China: A Retrospective and  
666 Prospects, *Int J Environ Res Public Health*, 13, 10.3390/ijerph13121219, 2016.
- 667 Kamens, R., Jang, M., Chien, C. J., and Leach, K.: Aerosol formation from the reaction of alpha-



- 668 pinene and ozone using a gas-phase kinetics aerosol partitioning model, *Environmental*  
669 *Science & Technology*, 33, 1430-1438, 1999.
- 670 Kan, H., Chen, R., and Tong, S.: Ambient air pollution, climate change, and population health in  
671 China, *Environ Int*, 42, 10-19, 10.1016/j.envint.2011.03.003, 2012.
- 672 Khoder, M. I.: Atmospheric conversion of sulfur dioxide to particulate sulfate and nitrogen dioxide  
673 to particulate nitrate and gaseous nitric acid in an urban area, *Chemosphere*, 49, 675-684, 2002.
- 674 Lelieveld, J., Evans, J. S., Fnais, M., Giannadaki, D., and Pozzer, A.: The contribution of outdoor  
675 air pollution sources to premature mortality on a global scale, *Nature*, 525, 367-371,  
676 10.1038/nature15371, 2015.
- 677 Li, L., Chen, C. H., Fu, J. S., Huang, C., Streets, D. G., Huang, H. Y., Zhang, G. F., Wang, Y. J.,  
678 Jang, C. J., Wang, H. L., Chen, Y. R., and Fu, J. M.: Air quality and emissions in the Yangtze  
679 River Delta, China, *Atmospheric Chemistry and Physics*, 11, 1621-1639, 10.5194/acp-11-  
680 1621-2011, 2011.
- 681 Li, L., Chen, C. H., Huang, C., Huang, H. Y., Zhang, G. F., Wang, Y. J., Wang, H. L., Lou, S. R.,  
682 Qiao, L. P., Zhou, M., Chen, M. H., Chen, Y. R., Streets, D. G., Fu, J. S., and Jang, C. J.: Process  
683 analysis of regional ozone formation over the Yangtze River Delta, China using the Community  
684 Multi-scale Air Quality modeling system, *Atmospheric Chemistry and Physics*, 12, 10971-  
685 10987, 2012.
- 686 Li, S. H., and Hong, H. P.: Typhoon wind hazard estimation for China using an empirical track  
687 model, *Natural Hazards*, 82, 1009-1029, 10.1007/s11069-016-2231-2, 2016.
- 688 Li, M., Liu, H., Geng, G., Hong, C., Liu, F., Song, Y., Tong, D., Zheng, B., Cui, H., Man, H., Zhang,  
689 Q., and He, K.: Anthropogenic emission inventories in China: a review, *National Science*  
690 *Review*, 4, 834-866, 10.1093/nsr/nwx150, 2017.
- 691 Li, M., Wang, T., Xie, M., Zhuang, B., Li, S., Han, Y., and Chen, P.: Impacts of aerosol-radiation  
692 feedback on local air quality during a severe haze episode in Nanjing megacity, eastern China,  
693 *Tellus B: Chemical and Physical Meteorology*, 69, 10.1080/16000889.2017.1339548, 2017.
- 694 Li, M., Wang, T., Xie, M., Zhuang, B., Li, S., Han, Y., Song, Y., and Cheng, N.: Improved  
695 meteorology and ozone air quality simulations using MODIS land surface parameters in the  
696 Yangtze River Delta urban cluster, China, *Journal of Geophysical Research: Atmospheres*, 122,  
697 3116-3140, 10.1002/2016jd026182, 2017.



- 698 Li, S., Wang, T., Huang, X., Pu, X., Li, M., Chen, P., Yang, X.-Q., and Wang, M.: Impact of East  
699 Asian Summer Monsoon on Surface Ozone Pattern in China, *Journal of Geophysical Research:*  
700 *Atmospheres*, 123, 1401-1411, 10.1002/2017jd027190, 2018.
- 701 Li, M., Wang, T., Xie, M., Li, S., Zhuang, B., Huang, X., Chen, P., Zhao, M., and Liu, J.: Formation  
702 and Evolution Mechanisms for Two Extreme Haze Episodes in the Yangtze River Delta Region  
703 of China During Winter 2016, *Journal of Geophysical Research: Atmospheres*, 124, 3607-3623,  
704 10.1029/2019jd030535, 2019.
- 705 Liao, J., Wang, T., Jiang, Z., Zhuang, B., Xie, M., Yin, C., Wang, X., Zhu, J., Fu, Y., and Zhang, Y.:  
706 WRF/Chem modeling of the impacts of urban expansion on regional climate and air pollutants  
707 in Yangtze River Delta, China, *Atmospheric Environment*, 106, 204-214,  
708 10.1016/j.atmosenv.2015.01.059, 2015.
- 709 Liao, Z., Gao, M., Sun, J., and Fan, S.: The impact of synoptic circulation on air quality and  
710 pollution-related human health in the Yangtze River Delta region, *The Science of the total*  
711 *environment*, 607-608, 838-846, 10.1016/j.scitotenv.2017.07.031, 2017.
- 712 Liu, D., Pang, L., and Xie, B.: Typhoon disaster in China: prediction, prevention, and mitigation,  
713 *Natural Hazards*, 49, 421-436, 10.1007/s11069-008-9262-2, 2009.
- 714 Liu, H., Liu, S., Xue, B. R., Lv, Z. F., Meng, Z. H., Yang, X. F., Xue, T., Yu, Q., and He, K. B.:  
715 Ground-level ozone pollution and its health impacts in China, *Atmospheric Environment*, 173,  
716 223-230, 2018.
- 717 Lou, S., Liao, H., and Zhu, B.: Impacts of aerosols on surface-layer ozone concentrations in China  
718 through heterogeneous reactions and changes in photolysis rates, *Atmospheric Environment*,  
719 85, 123-138, 10.1016/j.atmosenv.2013.12.004, 2014.
- 720 Lu, X., Hong, J., Zhang, L., Cooper, O. R., Schultz, M. G., Xu, X., Wang, T., Gao, M., Zhao, Y., and  
721 Zhang, Y.: Severe Surface Ozone Pollution in China: A Global Perspective, *Environmental*  
722 *Science & Technology Letters*, 5, 487-494, 10.1021/acs.estlett.8b00366, 2018.
- 723 Monks, P. S., Archibald, A. T., Colette, A., Cooper, O., Coyle, M., Derwent, R., Fowler, D., Granier,  
724 C., Law, K. S., Mills, G. E., Stevenson, D. S., Tarasova, O., Thouret, V., von Schneidmesser,  
725 E., Sommariva, R., Wild, O., and Williams, M. L.: Tropospheric ozone and its precursors from  
726 the urban to the global scale from air quality to short-lived climate forcer, *Atmospheric*  
727 *Chemistry and Physics*, 15, 8889-8973, 10.5194/acp-15-8889-2015, 2015.



- 728 Shu, L., Xie, M., Wang, T., Gao, D., Chen, P., Han, Y., Li, S., Zhuang, B., and Li, M.: Integrated  
729 studies of a regional ozone pollution synthetically affected by subtropical high and typhoon  
730 system in the Yangtze River Delta region, China, *Atmospheric Chemistry and Physics*, 16,  
731 15801-15819, 10.5194/acp-16-15801-2016, 2016.
- 732 Shu, L., Xie, M., Gao, D., Wang, T., Fang, D., Liu, Q., Huang, A., and Peng, L.: Regional severe  
733 particle pollution and its association with synoptic weather patterns in the Yangtze River Delta  
734 region, China, *Atmospheric Chemistry and Physics*, 17, 12871-12891, 10.5194/acp-17-12871-  
735 2017, 2017.
- 736 Tang, X.Y., Li, J.L., Dong, Z.X., Wang, Y.Y., Wang, W.X., Qi, L.W., Liu, X.L., Zhang, Y.T., Zhang,  
737 X.J., Tian, B.S., Jin, S.W., Yang, L.Q., Zhang, Y.X., 1989. Photochemical pollution in Lanzhou,  
738 China - a case study. *J. Environ. Sci. China* 1, 31e38.
- 739 Van Dingenen, R., Dentener, F. J., Raes, F., Krol, M. C., Emberson, L., and Cofala, J.: The global  
740 impact of ozone on agricultural crop yields under current and future air quality legislation,  
741 *Atmospheric Environment*, 43, 604-618, 10.1016/j.atmosenv.2008.10.033, 2009.
- 742 Voorhees, A. S., Wang, J., Wang, C., Zhao, B., Wang, S., and Kan, H.: Public health benefits of  
743 reducing air pollution in Shanghai: a proof-of-concept methodology with application to  
744 BenMAP, *The Science of the total environment*, 485-486, 396-405,  
745 10.1016/j.scitotenv.2014.03.113, 2014.
- 746 Wang, T., and Kwok, J. Y. H.: Measurement and analysis of a multiday photochemical smog episode  
747 in the Pearl River delta of China, *J Appl Meteorol*, 42, 404-416, 2003.
- 748 Wang, X., Zhang, Y., Hu, Y., Zhou, W., Lu, K., Zhong, L., Zeng, L., Shao, M., Hu, M., and Russell,  
749 A. G.: Process analysis and sensitivity study of regional ozone formation over the Pearl River  
750 Delta, China, during the PRIDE-PRD2004 campaign using the Community Multiscale Air  
751 Quality modeling system, *Atmospheric Chemistry and Physics*, 10, 4423-4437, 10.5194/acp-  
752 10-4423-2010, 2010.
- 753 Wang, M., Cao, C., Li, G., and Singh, R. P.: Analysis of a severe prolonged regional haze episode  
754 in the Yangtze River Delta, China, *Atmospheric Environment*, 102, 112-121,  
755 10.1016/j.atmosenv.2014.11.038, 2015.
- 756 Wang, T., Xue, L., Brimblecombe, P., Lam, Y. F., Li, L., and Zhang, L.: Ozone pollution in China:  
757 A review of concentrations, meteorological influences, chemical precursors, and effects, *The*



- 758 Science of the total environment, 575, 1582-1596, 10.1016/j.scitotenv.2016.10.081, 2017.
- 759 Wang, T., Gao, T., Zhang, H., Ge, M., Lei, H., Zhang, P., Zhang, P., Lu, C., Liu, C., Zhang, H.,  
760 Zhang, Q., Liao, H., Kan, H., Feng, Z., Zhang, Y., Qie, X., Cai, X., Li, M., Liu, L., and Tong,  
761 S.: Review of Chinese atmospheric science research over the past 70 years: Atmospheric  
762 physics and atmospheric environment, Science China Earth Sciences, 62, 1903-1945,  
763 10.1007/s11430-019-9536-1, 2019.
- 764 Wei, X., Lam, K.-s., Cao, C., Li, H., and He, J.: Dynamics of the Typhoon Haitang Related High  
765 Ozone Episode over Hong Kong, Advances in Meteorology, 2016, 1-12,  
766 10.1155/2016/6089154, 2016.
- 767 Xie, M., Zhu, K., Wang, T., Yang, H., Zhuang, B., Li, S., Li, M., Zhu, X., and Ouyang, Y.:  
768 Application of photochemical indicators to evaluate ozone nonlinear chemistry and pollution  
769 control countermeasure in China, Atmospheric Environment, 99, 466-473,  
770 10.1016/j.atmosenv.2014.10.013, 2014.
- 771 Xie, M., Liao, J., Wang, T., Zhu, K., Zhuang, B., Han, Y., Li, M., and Li, S.: Modeling of the  
772 anthropogenic heat flux and its effect on regional meteorology and air quality over the Yangtze  
773 River Delta region, China, Atmospheric Chemistry and Physics, 16, 6071-6089, 10.5194/acp-  
774 16-6071-2016, 2016.
- 775 Xie, M., Zhu, K., Wang, T., Chen, P., Han, Y., Li, S., Zhuang, B., and Shu, L.: Temporal  
776 characterization and regional contribution to O<sub>3</sub> and NO<sub>x</sub> at an urban and a suburban site in  
777 Nanjing, China, The Science of the total environment, 551-552, 533-545,  
778 10.1016/j.scitotenv.2016.02.047, 2016.
- 779 Xie, M., Shu, L., Wang, T.-j., Liu, Q., Gao, D., Li, S., Zhuang, B.-l., Han, Y., Li, M.-m., and Chen,  
780 P.-l.: Natural emissions under future climate condition and their effects on surface ozone in the  
781 Yangtze River Delta region, China, Atmospheric Environment, 150, 162-180,  
782 10.1016/j.atmosenv.2016.11.053, 2017.
- 783 Xu, X., Lin, W., Wang, T., Yan, P., Tang, J., Meng, Z., and Wang, Y.: Long-term trend of surface  
784 ozone at a regional background station in eastern China 1991-2006: enhanced variability,  
785 Atmospheric Chemistry and Physics, 8, 2595-2607, 2008.
- 786 Xue, L. K., Wang, T., Gao, J., Ding, A. J., Zhou, X. H., Blake, D. R., Wang, X. F., Saunders, S. M.,  
787 Fan, S. J., Zuo, H. C., Zhang, Q. Z., and Wang, W. X.: Ground-level ozone in four Chinese



788 cities: precursors, regional transport and heterogeneous processes, *Atmospheric Chemistry and*  
789 *Physics*, 14, 13175-13188, 10.5194/acp-14-13175-2014, 2014.

790 Yang, J. X., Lau, A. K. H., Fung, J. C. H., Zhou, W., and Wenig, M.: An air pollution episode and  
791 its formation mechanism during the tropical cyclone Nuri's landfall in a coastal city of south  
792 China, *Atmospheric Environment*, 54, 746-753, 10.1016/j.atmosenv.2011.12.023, 2012.

793 Ying, M., Zhang, W., Yu, H., Lu, X., Feng, J., Fan, Y., Zhu, Y., and Chen, D.: An Overview of the  
794 China Meteorological Administration Tropical Cyclone Database, *Journal of Atmospheric and*  
795 *Oceanic Technology*, 31, 287-301, 10.1175/jtech-d-12-00119.1, 2014.

796 Zhan, C.-c., Xie, M., Fang, D.-x., Wang, T.-j., Wu, Z., Lu, H., Li, M.-m., Chen, P.-l., Zhuang, B.-l.,  
797 Li, S., Zhang, Z.-q., Gao, D., Ren, J.-y., and Zhao, M.: Synoptic weather patterns and their  
798 impacts on regional particle pollution in the city cluster of the Sichuan Basin, China,  
799 *Atmospheric Environment*, 208, 34-47, 10.1016/j.atmosenv.2019.03.033, 2019.

800 Zhang, Q. A., Wu, L. G., and Liu, Q. F.: Tropical Cyclone Damages in China 1983-2006, *Bulletin*  
801 *of the American Meteorological Society*, 90, 489-+, 2009.

802 Zhao, C., Wang, Y., Yang, Q., Fu, R., Cunnold, D., and Choi, Y.: Impact of East Asian summer  
803 monsoon on the air quality over China: View from space, *Journal of Geophysical Research*,  
804 115, 10.1029/2009jd012745, 2010.

805 Zhao, K., Li, X., Xue, M., Jou, B. J.-D., and Lee, W.-C.: Short-term forecasting through intermittent  
806 assimilation of data from Taiwan and mainland China coastal radars for Typhoon Meranti  
807 (2010) at landfall, *Journal of Geophysical Research: Atmospheres*, 117, n/a-n/a,  
808 10.1029/2011jd017109, 2012.

809